Organic Electronics 15 (2014) 1521–1530

Contents lists available at ScienceDirect

Organic Electronics

journal homepage: www.elsevier.com/locate/orgel

Two-dimensional π-conjugated molecules based-on 2,6,9,10-tetra(prop-1-yn-1-yl)anthracene and their application to solution-processed photovoltaic cells

Jicheol Shin [a], Nam Su Kang [b,c], Tae Wan Lee [a], Min Ju Cho [a], Jae Min Hong [b], Byeong-Kwon Ju [c], Dong Hoon Choi [a,*]

[a] Department of Chemistry, Research Institute for Natural Sciences, Korea University, 5 Anam-dong, Sungbuk-gu, Seoul 136-701, Republic of Korea
[b] Future Convergence Research Division, Korea Institute of Science and Technology, P.O. Box 131, Cheongryang, Seoul 130-650, Republic of Korea
[c] Display and Nanosystem Laboratory, College of Engineering, Korea University, 145 Anam-ro, Seongbuk-gu, Seoul 136-713, Republic of Korea

ARTICLE INFO

Article history:
Received 1 December 2013
Received in revised form 8 April 2014
Accepted 8 April 2014
Available online 26 April 2014

Keywords:
Organic semiconductor
Tetra(prop-1-yn-1-yl)anthracene
Substitution position
Thin film transistor
Bulk heterojunction
Photovoltaic cell

ABSTRACT

Novel two-dimensional π-conjugated molecules, i.e., 5′,5‴-((9,10-bis((4-hexylphenyl)ethynyl)anthracene-2,6-diyl)bis(ethyne-2,1-diyl))bis(5-hexyl-2,2′-bithiophene) (2,6-HBT) and 5′,5‴-((2,6-bis((4-hexylphenyl)ethynyl)anthracene-9,10-diyl)bis(ethyne-2,1-diyl))bis(5-hexyl-2,2′-bithiophene) (9,10-THB) were successfully synthesized and utilized as highly soluble p-type organic semiconductors for organic thin film transistors (TFTs) and solar cells. From the TFTs, the high hole mobility of the pristine film of 9,10-THB was measured to be 0.07 $cm^2 V^{-1} s^{-1}$ ($I_{on/off} = 10^6$–10^7), which is mainly attributed to slip-stacked charge-transport behavior in J-aggregation-induced crystallites. Further, a solution-processed solar cell made of 9,10-THB and $PC_{61}BM$ exhibited very promising and reproducible power conversion efficiencies of 3.30% and 2.53% with composition 1:1 and 1:2 w/w ratio, respectively.

1. Introduction

The advantages of organic photovoltaic (OPV) cells, namely low cost, light weight, and high mechanical flexibility together with their high potential as a competitive technology to supply green energy has resulted in intensive research on OPVs [1–6]. Several researchers devoted great effort to develop highly efficient small molecules (SMs) and π-conjugated polymers to improve the power conversion efficiency (PCE) of solar cells. Additionally, various device structures are postulated to improve the performance of organic solar cells. Amongst the various types of p-type organic semiconducting materials, π-conjugated SMs are of particular interest because it is relatively easy to tune their electronic properties during their synthesis and purification; moreover, the performance of the corresponding PV devices is very stable and reproducible.

Recently, owing to the abovementioned advantages, solution-processed organic solar cells based on bulk-heterojunction (BHJ) systems have become a competitive alternative to conjugated-polymer-based solar cells [7–11]. The performance of SM-OPV has improved dramatically with the PCE ~7.0–9.0%, mostly by using low-band-gap molecules in the BHJ-type solar cells [12,13]. Such highly efficient OPVs were usually designed by employing low-band-gap materials that contain electron-rich (D) and electron-deficient (A) units, connected through a conjugated bond in a push–pull manner [14–18]. In contrast, not many low-band-gap conjugated molecules containing only donor moieties were reported that show promising device efficiency in BHJ-type solar cells.

* Corresponding author. Tel.: +82 2 3290 3140; fax: +82 2 924 3141.
E-mail address: dhchoi8803@korea.ac.kr (D.H. Choi).

http://dx.doi.org/10.1016/j.orgel.2014.04.021
1566-1199/

Fused acenes such as anthracene, tetracene, pentacene and pyrene were reported to show very promising charge-transport properties as good p-type semiconducting materials in organic field effect transistors (OFETs). Concomitantly, the various derivatives of fused acenes were also demonstrated to show an unusual interaction between molecules or between polymer chains, which exhibited broad absorption bands that fitted well to the solar emission spectrum. In the solid state, the absorption properties of the active materials were strongly dependent on the type and position of the substituent on the fused ring structure [19–24].

Among the various fused ring-structured moieties, anthracene is particularly attractive because of easy extension of its π-conjugated substituents in a two-dimensional way, good solubility, and unique crystallinity. However, irrespective of the great work done on anthracene-based OPV cells by solution processing, previous studies only displayed relatively low PCE values [19,25,26].

To enhance the performance of organic thin film transistors (TFTs) and solar cells using anthracene-based molecules, in addition to the compositions of D and A, miscibility, and internal morphology of the solid films, strategies for the structural design of p-type semiconducting molecules are important. Anthracene possesses four reactive positions—the 2,6- and 9,10-positions—to which the π-conjugated substituents are easily anchored [27–29]. However, when anchoring π-extended moieties to the 2,6- or 9,10-positions of the anthracene ring by single bonds, the molecular structures are highly twisted because of undesired steric hindrance of the 1-,3-, and 8-positions, resulting in the formation of a less-conjugated molecule [30–32] (Fig. 1(a)). In contrast, using triple bonds to attach the substituents to the anthracene ring can suppress the detrimental effect of the steric hindrance on molecular conjugation, as shown in Fig. 1(b).

In this work, we designed and synthesized new p-type anthracene-based molecules bearing 2,6,9,10-tetra(prop-1-yn-1-yl)anthracene (Scheme 1). We focused on the optical and photophysical properties of the molecules with respect to only the substituent position of alkyl-bithiophene to the anthracene molecule. In addition, to precisely understand the importance of the substitution position, the electrical properties of the molecules were investigated by fabricating TFT devices in order to compare the charge carrier mobility. 5′,5‴-((2,6-Bis((4-hexylphenyl)ethynyl)anthracene-9,10-diyl)bis(ethyne-2,1-diyl))bis(5-hexyl-2,2′-bithiophene) (9,10-THB) bearing J-aggregated crystalline structures exhibited a much higher carrier mobility than 5′,5‴-((9,10-bis((4-hexylphenyl)ethynyl)anthracene-2,6-diyl) bis(ethyne-2,1-diyl))bis(5-hexyl-2,2′-bithiophene) (2,6-HBT). The BHJ-type solar cell devices were fabricated with 2,6-HBT, 9,10-THB and $PC_{61}BM$. The device performance obtained from 9,10-THB bearing hexyl bithiophenes on the 9,10-positions of the anthracene ring displayed highly promising power conversion efficiencies of ~1.5–3.3% with the composition of the binary blend.

2. Experimental section

2.1. Materials

All chemicals were obtained from Sigma–Aldrich, Acros, and TCI and used without further purification. All the reactions and manipulations carried out under N_2 (g) was done using the standard inert-atmosphere equipment and Schlenk techniques, unless otherwise stated. Solvents used in the inert-atmosphere reactions were dried and degassed using standard procedures. Flash column chromatography was carried out with 230–400 mesh silica gel from Sigma–Aldrich by the wet-packing method. All deuterated solvents were purchased from Cambridge Isotope Laboratories, Inc. 2,6-Bis((4-hexylphenyl)ethynyl)anthracene-9,10-dione (1), 2,6-dibromo-9,10-bis((4-hexylphenyl)ethynyl)anthracene (2), and 5-ethynyl-5′-hexyl-2,2′-bithiophene (3) were synthesized by following previously published methods [33].

2.2. Synthesis

2.2.1. 5′,5‴-((2,6-Bis((4-hexylphenyl)ethynyl)anthracene-9,10-diyl)bis(ethyne-2,1-diyl))bis(5-hexyl-2,2′-bithiophene) (9,10-THB)

5-Ethynyl-5′-hexyl-2,2′-bithiophene (3; 1.0 g; 4.1 mmol) was dissolved in freshly distilled tetrahydrofuran (THF, 100 mL) in a 250-mL, oven-dried, magnetically stirred

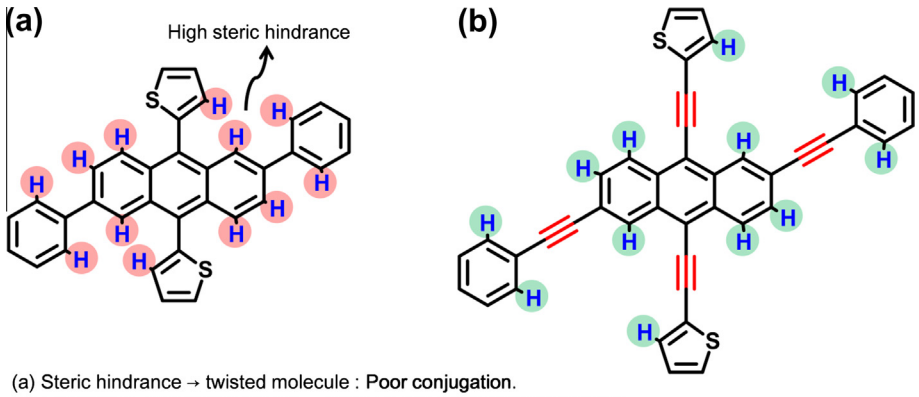

Fig. 1. Strategy for designing two-dimensional π-conjugated anthracene molecule.

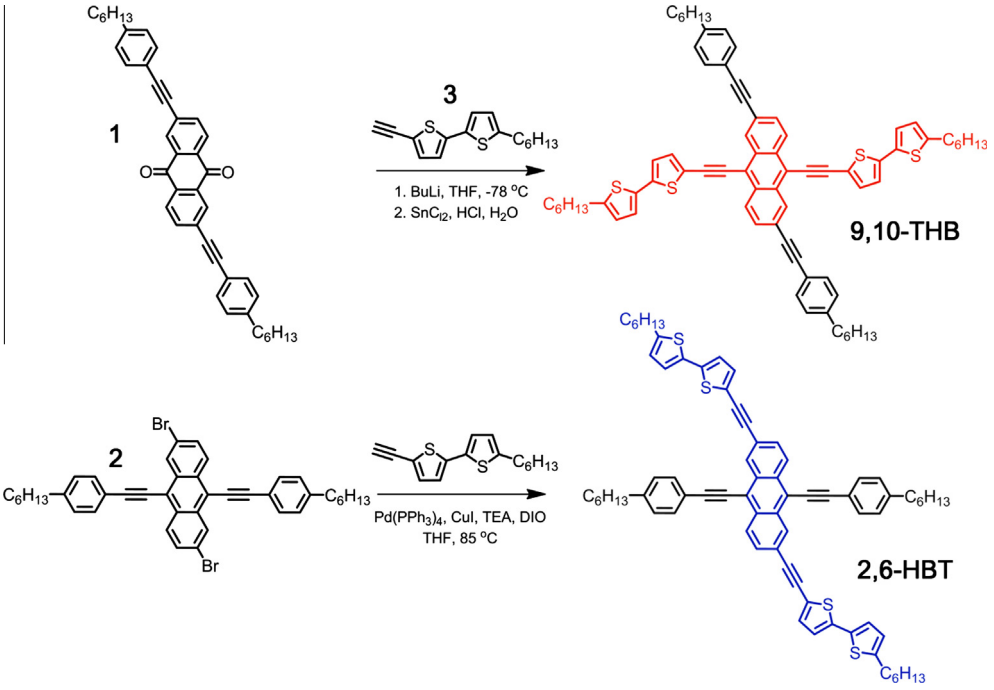

Scheme 1. Synthetic route for preparation of two anthracene-based molecules.

round-bottom flask (RBF). The solution was cooled to −78 °C, followed by the drop-wise addition of *n*-BuLi (1.7 mL, 12.3 mmol, 2.5 M solution in THF) for 5 min. The mixture was stirred for 30 min after which 2,6-bis((4-hexylphenyl)ethynyl)anthracene-9,10-dione (1; 0.8 g; 1.4 mmol) was added at −78 °C. The mixture was kept at room temperature for 3 h, and then quenched with water, $SnCl_2$, and HCl. After completing the workup, the resulting solution was poured into methanol and the precipitate was collected. The crude solid was purified by recrystallization from methanol. Yield 1.2 g, 80%. ^{1}H NMR (400 MHz, $CDCl_3$): δ (ppm) 8.69 (s, 2H), 8.52 (d, J = 9.0 Hz, 2H), 7.69 (d, J = 9.0 Hz, 2H), 7.57 (d, J = 8.2 Hz, 4H), 7.42 (d, J = 3.5 Hz, 2H), 7.22 (d, J = 8.2 Hz, 4H), 7.09 (t, J = 4.3 Hz, 2H), 6.73 (d, J = 3.5 Hz, 2H), 2.82 (t, 4H), 2.64 (t, 4H), 1.72–1.62 (m, 8H), 1.37–1.32 (m, 24H), 0.90 (m, 12H). ^{13}C NMR (100 MHz, $CDCl_3$): δ(ppm) 151.26, 148.71, 142.81, 135.14, 133.84, 132.79, 131.45, 130.54, 129.65, 126.26, 124.64, 124.44, 123.29, 122.85, 122.05, 121.37, 121.04, 120.62, 118.05, 96.89, 93.37, 91.21, 85.94, 31.73, 30.46, 30.51, 29.12, 22.79, 14.33. HRMS (EI) m/z (M^+): Calcd. for C74H74S4, 1091.64; found, 1091.85. Anal. Calcd. for $C_{74}H_{74}S_4$: C, 81.42; H, 6.83; S, 11.75 found: C, 81.54; H, 6.80; S, 11.66.

2.2.2. 5′,5‴-((9,10-Bis((4-hexylphenyl)ethynyl)anthracene-2,6-diyl)bis(ethyne-2,1-diyl))bis(5-hexyl-2,2′-bithiophene) (2,6-HBT)

2,6-Dibromo-9,10-bis((4-hexylphenyl)ethynyl)anthracene (2; 1 g; 1.5 mmol), bis(triphenylphosphine)palladium(II) dichloride (0.06 g, 0.075 mmol), and copper(I) iodide (0.015 g, 0.075 mmol) were dissolved in freshly distilled THF (25 mL), triethylamine (25 mL), and diisopropylamine (10 mL). 5-Ethynyl-5′-hexyl-2,2′-bithiophene (3; 1.23 g; 4.5 mmol) was added to the reaction mixture and heated at 85 °C for 16 h. After completing the reaction, the solution was poured into methanol and the precipitate was collected. The crude solid was purified by recrystallization from acetone. Yield 0.98 g, 62%. ^{1}H NMR(400 MHz, $CDCl_3$): δ (ppm) 8.68 (s, 2H), 8.53 (d, J = 9.0 Hz, 2H), 7.69 (d, J = 9.0 Hz, 2H), 7.58 (d, J = 8.2 Hz, 4H), 7.42 (d, J = 3.5 Hz, 2H), 7.23 (d, J = 8.2 Hz, 4H), 7.08 (t, J = 4.3 Hz, 2H), 6.72 (d, J = 3.5 Hz, 2H), 2.81 (t, 4H), 2.63 (t, 4H), 1.72–1.61 (m, 8H), 1.36–1.30 (m, 24H), 0.91 (m, 12H). ^{13}C NMR (100 MHz, $CDCl_3$): δ (ppm) 151.28, 148.70, 142.81, 135.13, 133.85, 132.81, 131.46, 130.56, 129.63, 126.25, 124.62, 124.44, 123.29, 122.85, 122.05, 121.37, 121.03, 120.62, 118.05, 96.88, 93.37, 91.21, 85.94, 31.72, 30.46, 30.51, 29.12, 22.78, 14.33. HRMS (EI) m/z (M^+): Calcd. for $C_{74}H_{74}S_4$, 1091.64; found, 1091.71. Anal. Calcd. For $C_{74}H_{74}S_4$: C, 81.42; H, 6.83; S, 11.75 found: C, 81.52; H, 6.84; S, 11.64.

2.3. Instrumental analysis

^{1}H NMR spectra were recorded on a Varian Mercury nuclear magnetic resonance (NMR) 400 MHz spectrometer using deuterated chloroform. ^{13}C NMR spectra were recorded using a Varian Inova-500 spectrometer. Elemental analyses were performed using an EA1112 (Thermo Electron Corp.) elemental analyzer. High resolution mass spectrometry (HRMS) analysis was performed on a JMS-700 MStation mass spectrometer (JEOL, resolution 60,000, m/z range at full sensitivity 2,400). Thermal properties were studied under a N_2 atmosphere on a Mettler DSC 821^e instrument (DSC, differential scanning calorimetry).

Thermogravimetric analysis (TGA) was conducted on a Mettler TGA50 (temperature rate 10 °C min^{-1} under N_2). The redox properties of the molecule were examined using cyclic voltammetry (CV) (Model: EA161 eDAQ). Thin films were coated on a Pt plate using chloroform as a solvent. The electrolyte solution employed was 0.10 M tetrabutylammonium hexafluorophosphate (Bu_4NPF_6) in freshly dried acetonitrile. Ag/AgCl and Pt wire (0.5 mm in diameter) electrodes were utilized as reference and counter electrodes, respectively, with a scan rate of 50 mV s^{-1}.

Atomic force microscopy (AFM, Advanced Scanning Probe Microscope, XE-100, PSIA) operating in the tapping mode with a silicon cantilever was used to characterize the surface morphologies of the thin films. The film sample was fabricated by spin-coating the chloroform solution on a *n*-octyltrichlorosilane (OTS)-treated silicon wafer, followed by drying at 50 °C under vacuum (solvent: chlorobenzene (CB), concentration: 30 mg mL^{-1}). The AFM images of the blend films for OPV were obtained from the thin films fabricated by spin-coating the CB solution on the poly(3,4-ethylenedioxythiophene) poly(styrenesulfonate) (PEDOT:PSS) layer on ITO glass.

In order to study the optical absorption behavior, thin films were fabricated on quartz substrates as follows: a chloroform solution (1 wt%) was filtered through an Acrodisc syringe filter (Millipore 0.45 μm, Millipore, Billerica, MA, USA), and subsequently spin-cast on quartz glass. The films were dried overnight at 60 °C for 12 h under vacuum. The absorption spectra of the samples as films (solvent: CB, concentration: 30 mg mL^{-1}) and as a solution (chloroform, concentration 1×10^{-6} mole L^{-1}) were obtained using a UV–vis absorption spectrometer (HP 8453, photodiode array type) in the wavelength range 190–1100 nm.

The grazing incidence X-ray diffraction (GI-XRD) measurements were performed at the 9A (U-SAXS) beam line (energy = 11.26 keV; pixel size = 79.6 μm; wavelength = 1.101 Å and the wide-angle X-ray diffraction (WAXD) measurements were performed at the 3C2 beam line (wavelength = 1.54 Å) at the Pohang Accelerator Laboratory (PAL)). The measurements were obtained over a scanning interval of 2θ between 0° and 20°. The variable q_{xy} (q_z) is the component of the scattering vector parallel (perpendicular) to the substrate, where $q = (4\pi/\lambda)\sin\theta$. The wavelength of the incident radiation is denoted by λ; θ is equal to half of the scattering angle. The film samples were fabricated by spin-casting on an OTS-treated silicon wafer, followed by drying at 50 °C under vacuum (solvent: CB, concentration: 30 mg mL^{-1}).

2.4. Fabrication of organic thin film transistor

To characterize the TFT performance, bottom gate top contact (BGTC) device geometry was employed. On a heavily *n*-doped SiO_2/Si substrate, the spin-coated films (thickness ~50–60 nm) of a molecule were prepared using chloroform as a solvent. Surface modification was carried out with OTS in order to ensure a hydrophobic dielectric surface. Source and drain electrodes for the TFT devices were then thermally evaporated (100 nm) through a shadow mask with a channel width and length of 1500 and 100 μm, respectively. The field effect mobility were calculated from the saturation regime from the relationship $\mu_{sat} = (2I_{DS}L)/(WC_i(V_G - V_{th})^2)$, where I_{DS} is the saturation drain current, C_i is the capacitance of the SiO_2 dielectric, V_G is the gate bias, and V_{th} is the threshold voltage. The device performance was evaluated in air using the 4200SCS semiconductor characterization system.

2.5. OPV device fabrication

The hole-collecting electrode was 150-nm-thick indium tin oxide (ITO) coated glass with a resistance of 15.0 Ω/cm. The ITO glass was cleaned in acetone, deionized water, and isopropyl alcohol by sonification for 30 min in each solvent. Finally, the cleaned ITO coated glass was dried in a vacuum oven for 2 h at 180 °C. Next, the cleaned ITO coated glass was treated with O_2 plasma and flattened with a microwave-generated plasma reactor (CR403 M, 90 W) for 10 min. A 50-nm-thick PEDOT:PSS layer (Baytron P) was coated on the ITO glass by spin coating from a stock solution of PEDOT:PSS and methanol (1:1, v/v) at 4000 rpm for 40 s. The PEDOT:PSS coating was thermally treated in a glove box at 100 °C for 30 min. The molecules (9,10-THB and 2,6-HBT) and $PC_{61}BM$ were dissolved in the anhydrous CB. The resulting solution was then spin-coated onto the PEDOT:PSS layer, followed by vacuum -drying the active layer at 60 °C for 6 h. The resulting photoactive layer was 100 nm thick and no additional thermal treatment was performed. To fabricate the electrode, 150-nm-thick aluminum was evaporated on a LiF thin layer. The current–voltage characteristics were measured with a Keithley 2400 source-measure unit. A 300-W Xe lamp was used as a light source to obtain an intensity of 100 mW cm^{-2}. To mimic sunlight, an AM 1.5 filter (Oriel) and a neutral density filter were used to reduce the intensity when necessary. Intensity of the incoming light power was measured with a calibrated broadband optical power meter (Spectra Physics model 404).

3. Results and discussion

3.1. Synthesis and property

The two p-type anthracene-based molecules were successfully synthesized by following the modified literature procedures [34,35]. As shown in Scheme 1, intermediate 3 was treated with *n*-BuLi and the resulting lithium salts reacted with 1, followed by reduction with $SnCl_2$ to afford 9,10-THB in a high yield of 80%. 2,6-HBT was prepared by a Sonogashira coupling reaction in a fairly high yield of 62%. The identity and purity of the synthetic products were confirmed by ^1H NMR, ^{13}C NMR, HRMS, and elemental analysis. The two anthracene molecules have exactly the same molecular weight and formula, but their conjugation pathways are different as they depend on the substituent position. In addition, variation in the electron density distributions at different positions was observed from the density functional theory (DFT) calculations (Fig. 2(b)). Four hexyl chains were substituted onto the benzene and bithiophene units as solubilizing and crystallization-promoting

groups. The two medium-sized molecules were found to have good self-film-forming properties and exhibited excellent solubility in common organic solvents such as chloroform, THF, dichloromethane, and CB.

The thermal properties of the molecules were characterized by DSC and TGA (see the measured data in Table 1). Compounds 9,10-THB and 2,6-HBT were thermally stable up to 400 °C. The DSC traces show that the melting points of 9,10-THB and 2,6-HBT are 165 and 152 °C, respectively.

3.2. Optical and electrochemical properties

The optical properties of the two molecules were investigated by UV–vis absorption spectroscopy. The absorption spectra measured from a dilute solution and thin films are shown in Fig. 2 and the measured parameters are summarized in Table 1. The solution spectrum of 9,10-THB exhibited a red shift ($\Delta\lambda$ = 43 nm) compared to that of 2,6-HBT. This shift is caused by the longer effective conjugation length along the 9,10-positions on the anthracene ring. Intriguingly, for 9,10-THB, a substantially high red shift ($\Delta\lambda$ = 118 nm) was observed upon film formation, which demonstrates strong intermolecular interactions between the molecules in the films. This large spectral red shift indicates that 9,10-THB possesses a well-organized molecular crystalline structure driven by the J-aggregation behavior in the film state, as was observed in our previous work [34,35]. The optical band gaps of 9,10-THB and 2,6-HBT were measured by using the absorption cut-off wavelength and are estimated to be 1.89 and 2.12 eV in the film states, respectively. 9,10-THB, with hexyl bithiophene units at the 9,10-positions, has a slightly lower band gap than 2,6-HBT, which proves that the substitution in the 9,10-positions can efficiently increase the conjugation length, molecular order, and crystallinity.

In addition, the blend film with 9,10-THB and $PC_{61}BM$ displayed absorption spectral behavior similar to that of the 9,10-THB film, thus maintaining the absorption maximum wavelength (λ_{max}). The sharp absorption band originating from 9,10-THB were highly persistent at 630 nm in all compositions (Fig. 2(C)). This indicates that the J-aggregation-induced crystalline structure of 9,10-THB in the blend film was robustly maintained, even when the $PC_{61}BM$ and 9,10-THB molecules were mixed together. In contrast, the absorbance of 2,6-HBT at approximately 500–550 nm decreased on adding $PC_{61}BM$ (Fig. 2(d)), which implies that the crystalline structure of 2,6-HBT was disrupted.

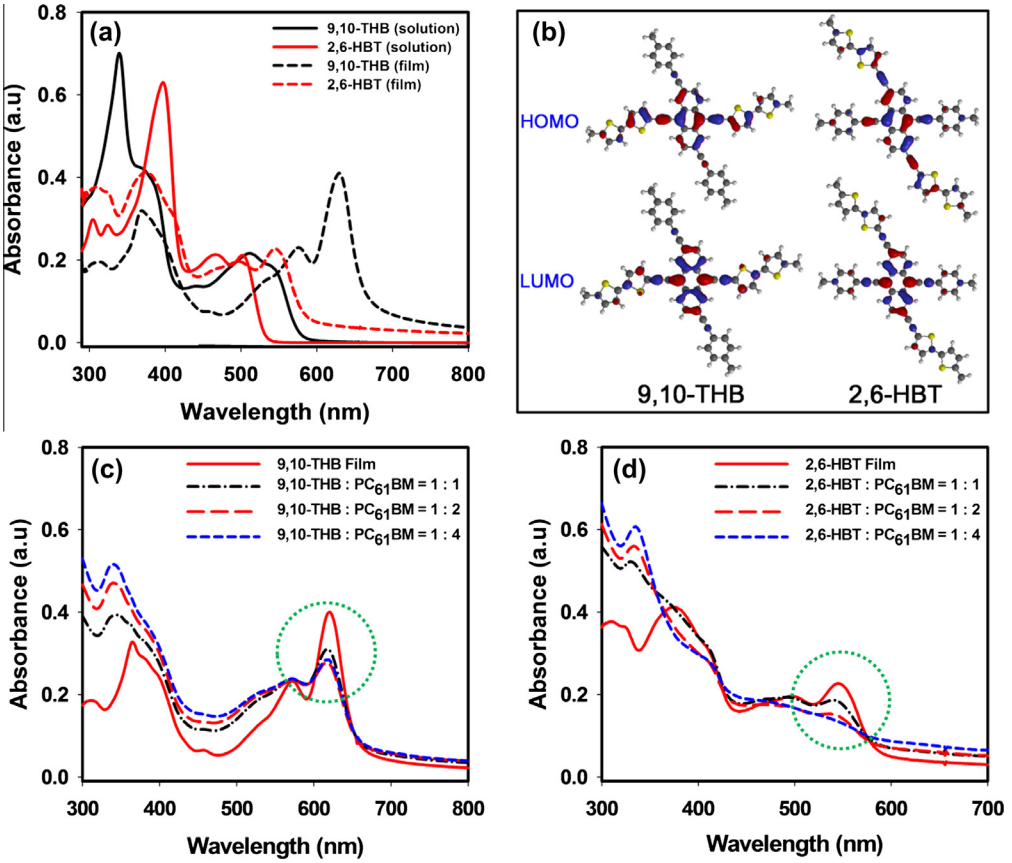

Fig. 2. (a) UV–vis absorption spectra of 9,10-THB and 2,6-HBT in solution and films. (b) Electron distribution calculated with density functional theory (DFT) calculations in HOMO and LUMO states. (c) Absorption spectra of blend films with 9,10-THB and $PC_{61}BM$, (d) Absorption spectra of blend films with 2,6-HBT and $PC_{61}BM$.

Table 1
Optical, thermal, and electrochemical properties of two anthracene molecules: 9,10-THB and 2,6-HBT.

Molecule	T_m	T_c	T_d	λ_{max}^{abs} (nm)[a]		$\lambda_{cut\ off}$	E_g^{opt}	E_{ox}^{onset}	HOMO	LUMO
	(°C)	(°C)	(°C)	Solution[a]	Film[b]	(mn)[c]	(eV)[c]	(eV)[d]	(eV)[d]	(eV)[c]
2,6-HBT	152	128	399	397,502	374,545	584	2.12	0.78	−5.59	−3.47
9,10-THB	165	148	399	340,512	369,630	655	1.89	0.60	−5.41	−3.52

[a] Measured in chloroform with a concentration of 10^{-5} M.
[b] Films were spin-coated from chloroform solution.
[c] Film state.
[d] The values were obtained from cyclic voltammograms. Sample: film on Pt electrode.

Electrochemical properties of the anthracene molecules were measured by CV to determine their HOMO energy level. To determine the LUMO energy level, the oxidation potential in CV was combined with the optical energy band gap (E_g^{opt}) resulting from the absorption edge in the absorption spectrum. Using these methods, the energy levels of HOMO and LUMO, which are −5.41 and −3.52 eV for 9,10-THB and −5.59 and −3.47 eV for 2,6-HBT, were calculated (Table 1). These results indicate that the substitution of hexyl bithiophene onto the 9,10-positions can tune the HOMO and LUMO levels because of the increased conjugation length. Consequently, 9,10-THB can display a low-band-gap energy of 1.89 eV only with an electron-donating moiety.

3.3. Organic thin film transistor performance

To investigate the effect of the substitution position on the charge-transport behavior, TFT devices (W = 1500 μm, L = 100 μm) were fabricated in a BGTC device configuration. The mobility was obtained from the source-drain current-gate voltage curves (I_{DS} versus V_G) at room temperature under ambient conditions without thermal annealing (Fig. 3). The OTFTs made with 9,10-THB and 2,6-HBT exhibited typical p-channel transistor behaviors without thermal annealing treatment. The mobility observed for the 2,6-HBT pristine films in TFTs was only 7.3×10^{-3} $cm^2\ V^{-1}\ s^{-1}$ ($I_{on/off} = 10^5$–10^6). In contrast, the 9,10-THB film exhibited relatively better charge-transport properties, showing mobility of approximately 0.07 $cm^2\ V^{-1}\ s^{-1}$ ($I_{on/off} = 10^6$–10^7). It was suggested that the HOMO energy levels of the semiconducting materials affect the threshold voltages of organic TFTs [36,37]. According to the CV measurement, 2,6-HBT has a lower HOMO level than 9,10-THB (−5.41 eV for 9,10-THB and −5.59 eV for 2,6-HBT in the film states). 2,6-HBT showed threshold voltage up to −21 V, whilst the threshold voltage of 9,10-THB is relatively less negative by −10 V. This result can possibly be explained by the reduction of the hole-injection barrier from the electrode to the active channel layer of 9,10-THB.

3.4. Characterization of binary blend films composed of anthracene-based molecules and $PC_{61}BM$

It is well known that the morphology of the photoactive material in BHJ solar cells substantially affects the device performance [38–40]. To understand the effect of the internal morphology of the photoactive layers on the photovoltaic performance, the morphological structures of the blend films of the anthracene-based molecules and $PC_{61}BM$ were studied using tapping mode atomic force microscopy (AFM) measurements. As can be seen in Fig. 4, the surface roughness of the 2,6-HBT:$PC_{61}BM$ (1:1 w/w ratio) and 9,10-THB:$PC_{61}BM$ (1:1 w/w ratio) blend films were 3.7 and 4.1 nm, respectively. In both the anthracene-based molecules and $PC_{61}BM$ blend films produced on decreasing the composition of $PC_{61}BM$, most of the large crystalline domains disappeared, and the blend films exhibited a smoother and more uniform surface. Consequently, the larger crystalline domains indicate a reduced interfacial contact area between the donor and acceptor molecules with poorer crystallite connectivity, resulting in lower photovoltaic performance [41,42]. The reduced surface roughness implied that the anthracene-based molecules and $PC_{61}BM$ formed smaller crystalline domains and the blend matrix might have a higher packing density, which can induce better charge transporting property on a nanoscopic scale. Additionally, the smoother surface may have facilitated a more intimate contact between the blend film and the electrodes, leading to the high J_{sc} values.

GI-XRD and WAXD was employed to obtain information about the crystalline morphological features within the pristine donor films and blend films [7,43–47]. The blend films were prepared under conditions similar to those used for solar cell fabrication with the corresponding GI-XRD patterns, as shown in Fig. 5. In the blend film with a 1:4 w/w ratio (2,6-HBT or 9,10-THB:$PC_{61}BM$), the anthracene-based molecules were randomly distributed and a large $PC_{61}BM$ scattering pattern could be observed, indicating no apparent molecular order with respect to the film surface. (See Fig. 5(a) and (e)) In contrast, anthracene-based molecule/$PC_{61}BM$ blend films with a 1:1 w/w ratio displayed improved packing and molecule order, which is attributed to the well-preserved crystallites (see Fig. 5(c) and (g)). By adding $PC_{61}BM$ into 2,6-HBT (1:1 wt ratio), the diffraction peak at 3.32° disappeared as can be seen in Fig. 5(d), which indicates that the crystalline domains of 2,6-HBT were destroyed by mixing with $PC_{61}BM$ molecules. On the contrary, The XRD pattern of the blend film of 9,10-THB and $PC_{61}BM$ (1:1 wt. ratio) displayed strong diffraction peak at 3.53° from the crystallites of 9,10-THB. (See Fig. 5(h)) It clearly revealed that the crystalline structure of 9,10-THB was maintained in the blend film even though $PC_{61}BM$ was added, which can enhance the charge transporting property in PV devices. These XRD analyses support, along with the results of UV–vis absorption

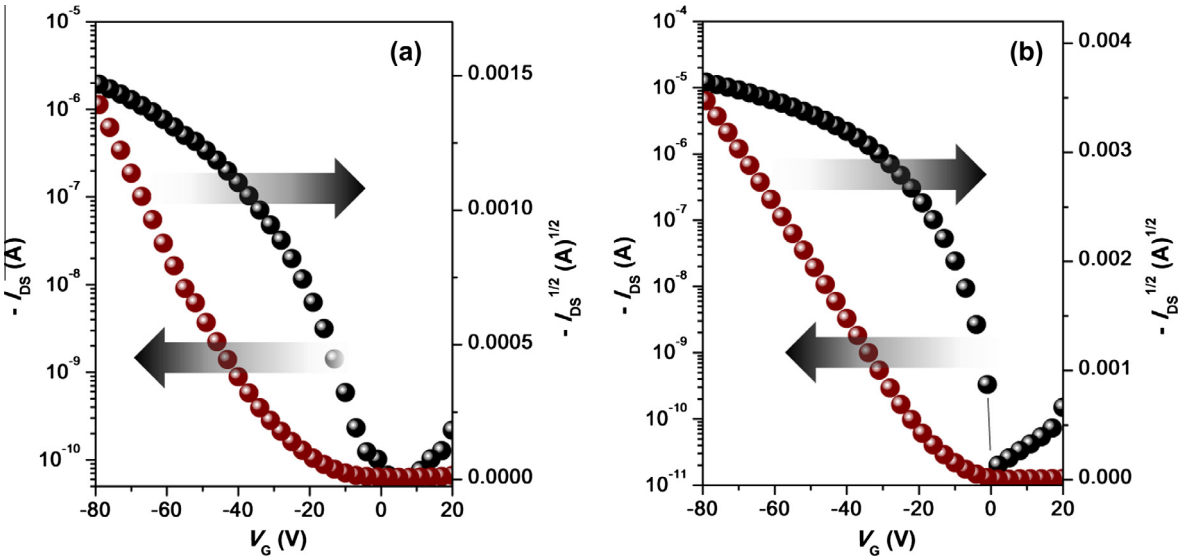

Fig. 3. Transfer characteristics of TFTs made from two anthracene-based molecules at $V_{DS} = -80$ V. (a) 2,6-HBT, (b) 9,10-THB.

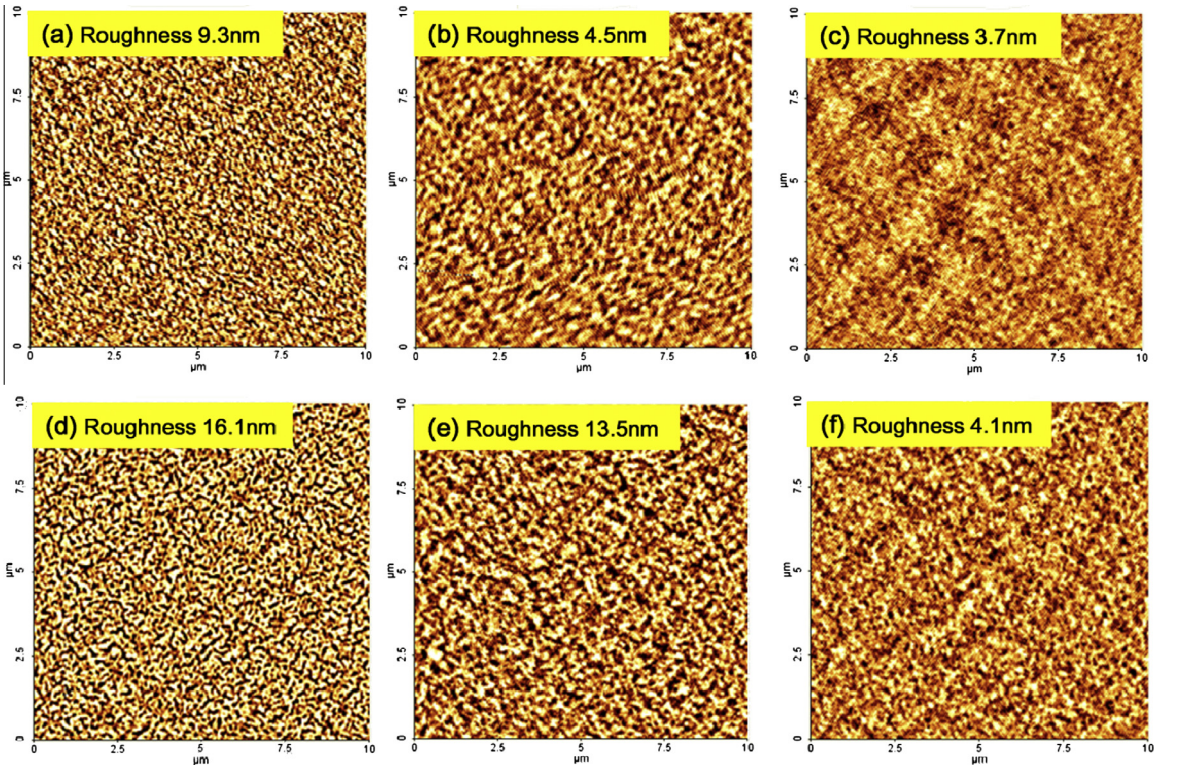

Fig. 4. (a–c): AFM images of 2,6-HBT/$PC_{61}BM$ blend films with a weight ratio of (a) 1:4, (b) 1:2, (c) 1:1; (d–f): AFM images of 9,10-THB /$PC_{61}BM$ blend films with a weight ratio of (d) 1:4, (e) 1:2, (f) 1:1.

spectroscopy, that the J-aggregation-induced crystalline structure of the anthracene-based molecule, 9,10-THB in the blend film could be maintained.

For modulating the PCE, charge carrier mobility is also related to the short circuit current, J_{sc}. Thus, the hole mobility of the blend films with the anthracene-based molecules and $PC_{61}BM$ were measured by the space-charge-limited current (SCLC) method, with a hole-only device structure of ITO/PEDOT:PSS/blend film/Au obtained in dark using the Mott–Gurney equation (Fig. 6) [48]. The mobility were calculated from $J = 98\varepsilon\varepsilon_o\mu V^2 d^3$, where J is the current density, V is the applied voltage, d is the

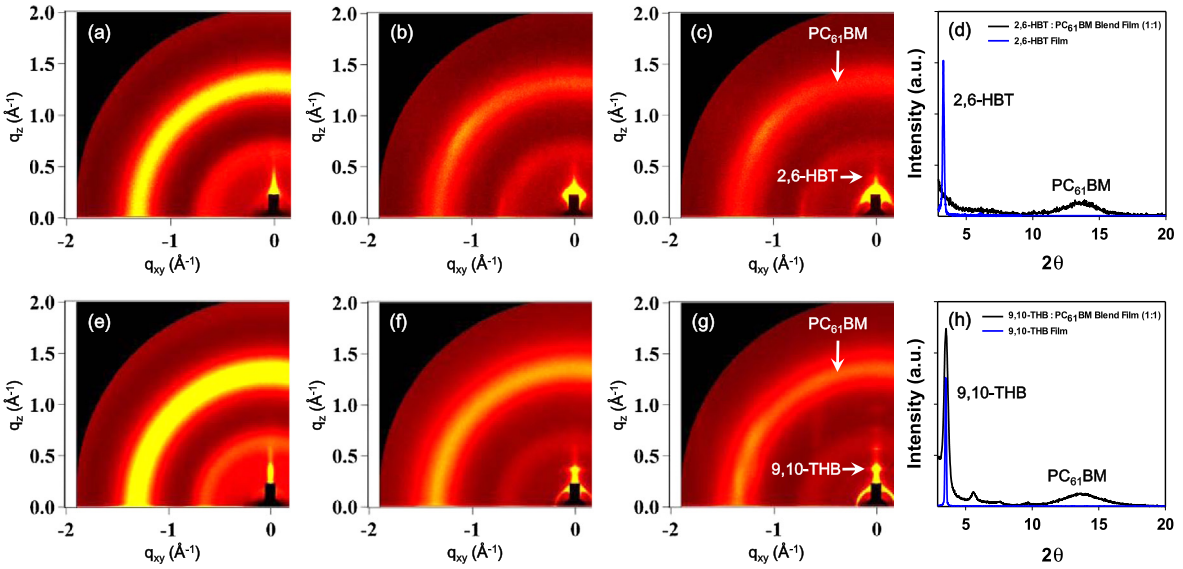

Fig. 5. (a–c): Two-dimensional GI-XRD patterns of blend films at the 2,6-HBT/$PC_{61}BM$ weight ratio of (a) 1:4, (b) 1:2, (c) 1:1. (e–g): Two-dimensional GI-XRD patterns of blend films at the 9,10-THB /$PC_{61}BM$ weight ratio of (e) 1:4, (f) 1:2, (g) 1:1. (d and h): XRD patterns of pristine films of 2,6-HBT and 9,10-THB, respectively. XRD patterns of the blend films were also included.

thickness of the blend film, $\varepsilon\varepsilon_o$ is the permittivity of the anthracene-based molecules:$PC_{61}BM$ blend films, μ is the hole mobility. The effective voltage (V) was calculated by substracting V_{bi} (built-in potential) and V_a (voltage drop due to PEDOT:PSS layer) from the applied voltage (V_{appl}). Since ITO and gold were used as electrode materials, the V_{bi} was assumed to be zero for simplicity. The voltage drop, V_a was calculated by using the resistance ($\sim$10 Ω) of PEDOT:PSS we employed for this device fabrication. The hole mobility of 2,6-HBT:$PC_{61}BM$ was calculated to be 1.8×10^{-5}, 2.3×10^{-5}, and 2.7×10^{-5} $cm^2\,V^{-1}\,s^{-1}$ at weight ratios of 1:1, 1:2, and 1:4, respectively. Whereas the hole mobility of 9,10-THB:$PC_{61}BM$ were calculated to be 1.4×10^{-4}, 5.9×10^{-5}, and 3.7×10^{-5} $cm^2\,V^{-1}\,s^{-1}$ at weight ratios of 1:1, 1:2, and 1:4, respectively (Fig. 6). Therefore, a higher J_{sc} value could be expected in the photovoltaic cells made from 9,10-THB:$PC_{61}BM$ than the device made from 2,6-HBT:$PC_{61}BM$.

3.5. Photovoltaic properties

The photovoltaic properties based on anthracene molecules were studied in BHJ solar cells using $PC_{61}BM$ as an acceptor. The device configuration was ITO/PEDOT:PSS/anthracene-based molecules: $PC_{61}BM$/LiF/Al. In particular, because the two anthracene-based molecules have the same molecular weight, the mole ratio of the blend film was identical between the anthracene-based molecules and $PC_{61}BM$, which makes it possible to compare their photovoltaic properties by only considering the effect of the different substituent position of hexyl bithiophene. The photoactive layers were spin-coated from CB solutions and the weight ratios of the anthracene-based molecules to $PC_{61}BM$ were selected to be 1:1, 1:2, and 1:4. The curves of current density versus voltage (J–V) measured from the blend samples under an AM 1.5 condition at 100 mW cm^{-2} are shown in Fig. 7. The best photovoltaic performance

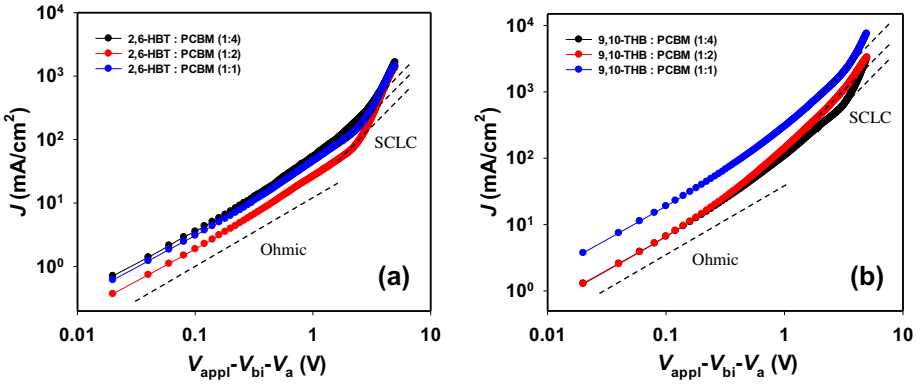

Fig. 6. J–V curves measured in dark to determine hole mobility of ITO/PEDOT/anthracene-based molecule:$PC_{61}BM$/Au device: (a) 2,6-HBT, (b) 9,10-THB.

with 2,6-HBT was obtained at a weight ratio of 1:1, with an open circuit voltage (V_{oc}) of 0.84 V, J_{sc} of 2.96 mA cm^{-2}, a fill factor (FF) of 0.44, and a PCE of 1.10%. In PV devices with 1:4 and 1:2 wt ratio of 2,6-HBT and $PC_{61}BM$, the shunt resistance might be relatively much smaller, which indicates the inhomogeneous photoactive layer and poor interfacial contact between photoactive layer and the electrode [21]. In contrast, using 9,10-THB instead of 2,6-HBT as a donor, the PCE value of the 9,10-THB-based solar cells became 3.30% with a V_{oc} of 0.82 V, a J_{sc} of 8.75 mA cm^{-2}, and an FF of 0.46 at a 1:1 weight ratio. Although the large energy difference between the HOMO of the 2,6-HBT and the LUMO of $PC_{61}BM$ is observed, the V_{oc} value of the 2,6-HBT device did not show large difference from that of 9,10-THB based device. This might be attributed to variation of internal morphology of blend film and poor interfacial contact between donor molecule and $PC_{61}BM$ [21,49,50]. The photovoltaic performance data compared to the blend composition is listed in Table 2. In Fig. 7(d), we can compare the external quantum efficiencies of the OPV cells fabricated with two different donors. As was expected, 2,6-HBT based devices exhibited much smaller EQE under an identical compositions than 9,10-THB based devices in the whole measured wavelength range. Intriguingly, 9,10-THB-based solar cells exhibited a maximum EQE at the range 550–650 nm, which is coincident with the absorption band of the J-aggregates in the absorption spectrum. Thus, owing to the robust maintenance of J-aggregated crystallites, the devices containing 9,10-THB and $PC_{61}BM$ exhibited better performance than the devices containing 2,6-HBT and $PC_{61}BM$ (Fig. 7(d)). These results prove that photoactive layers that absorb more of the available photons from a broad range of the optical spectrum enhanced the device photocurrent, which is consistent with high J_{sc} values and an improvement in the device performance. In brief, our results unambiguously demonstrated the effect of alkyl-bithiophene to the anthracene molecule on the power conversion efficiency in bulk heterojunction PV cells with $PC_{61}BM$.

4. Conclusions

In conclusion, two SMs, 2,6-HBT and 9,10-THB, according to the substituent position of alkyl-bithiophene as the only p-type semiconductor have been designed and synthesized. 2,6-HBT exhibited carrier mobility of 7.3 × 10^{-3} cm^2 V^{-1} s^{-1} in TFTs, whereas 9,10-THB showed an improved charge-transport property and the carrier

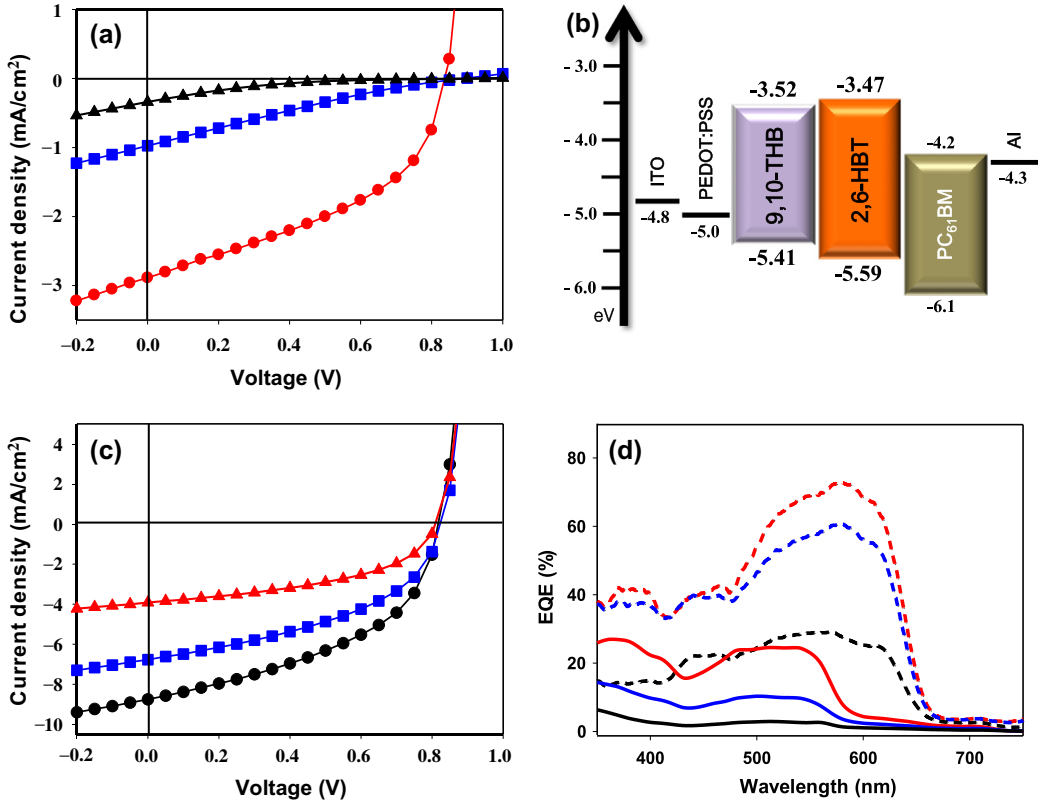

Fig. 7. Current density–voltage (*J*–*V*) characteristics of OPVs based on (a) 2,6-HBT:$PC_{61}BM$ and (c) 9,10-THB:$PC_{61}BM$ active layers with three blend compositions. *circle (donor: $PC_{61}BM$ = 1:1), square (1:2), triangle (1:4). (b) Device configuration and HOMO and LUMO energy diagram of 2,6-HBT and 9,10-THB. (d) External quantum efficiencies (EQEs) of PV cells. *Solid line (2,6-HBT:$PC_{61}BM$); Dashed line (9,10-THB:$PC_{61}BM$); Red line: (1:1); Blue line: (1:2); Green line: (1:4). (For interpretation of the references to colour in this figure legend, the reader is referred to the web version of this article.)

Table 2
Photovoltaic properties of different blend compositions of 2,6-HBT:$PC_{61}BM$ and 9,10-THB:$PC_{61}BM$ solar cells.

Composition of blend film	V_{oc} (V)	J_{sc} (mA/cm^2)	FF	PCE (%)
2,6-HBT:$PC_{61}BM$(1:1)	0.84	−2.96	0.44	1.10
2,6-HBT:$PC_{61}BM$(1:2)	0.88	−0.97	0.21	0.18
2,6-HBT:$PC_{61}BM$(1:4)	0.89	−0.34	0.12	0.03
9,10-THB:$PC_{61}BM$(1:1)	0.82	−8.75	0.46	3.30
9,10-THB:$PC_{61}BM$(1:2)	0.83	−6.77	0.45	2.53
9,10-THB:$PC_{61}BM$(1:4)	0.81	−3.92	0.48	1.52

mobility of 0.07 cm^2 V^{-1} s^{-1}, which has been attributed to strong specific intermolecular interaction. 9,10-THB also exhibits a substantially red-shifted absorption spectrum and broadening of the absorption wavelength range. These intriguing features in the solid-state films generate a higher photocurrent than the 2,6-HBT in blend films; as a result, the encouraging PCE of 3.30% was achieved in a BHJ film fabricated with the 9,10-THB/$PC_{61}BM$ (1:1 w/w ratio) blend, without thermal annealing. It was conclusively found in this study that intriguingly robust J-aggregates in 9,10-THB crystallites provide advantages for enhancing charge transporting property in TFT devices and photocurrent in PV devices.

Acknowledgments

This research was supported by National Research Foundation of Korea (NRF2012R1A2A1A01008797) and by Key Research Institute Program through the NRF funded by the Ministry of Education, Science and Technology (NRF20120005860). We are grateful to Pohang Accelerator Laboratory (Pohang, Korea) for allowing us to conduct the GI-XRD measurements.

References

[1] W. Tang, J. Hai, Y. Dai, Z. Huang, B. Lu, F. Yuan, J. Tang, F. Zhang, Sol. Energy Mater. Sol. Cells 94 (2010) 1963.
[2] N.S. Lewis, Science 315 (2007) 798.
[3] F.C. Krebs, S.A. Gevorgyan, J. Alstrup, J. Mater. Chem. 19 (2009) 5442.
[4] E. Kymakis, K. Savva, M.M. Stylianakis, C. Fotakis, E. Stratakis, Adv. Funct. Mater. 23 (2013) 2742.
[5] J. Jin, J. Lee, S. Jeong, S. Yang, J.-H. Ko, H.-G. Im, S.-W. Baek, J.-Y. Lee, B.-S. Bae, Energy Environ. Sci. 6 (2013) 1811.
[6] J.-H. Lee, H.-S. Shin, S.-I. Na, H.-K. Kim, Sol. Energy Mater. Sol. Cells 109 (2013) 192–198.
[7] O.P. Lee, A.T. Yiu, P.M. Beaujuge, C.H. Woo, T.W. Holcombe, J.E. Millstone, J.D. Douglas, M.S. Chen, J.M.J. Fréchet, Adv. Mater. 23 (2011) 5359.
[8] L.-C. Chi, H.-F. Chen, W.-Y. Hung, Y.-H. Hsu, P.-C. Feng, S.-H. Chou, Y.-H. Liu, K.-T. Wong, Sol. Energy Mater. Sol. Cells 109 (2013) 33.
[9] Y. Liu, Y. Michael Yang, C.-C. Chen, Q. Chen, L. Dou, Z. Hong, G. Li, Y. Yang, Adv. Mater. 25 (2013) 4657.
[10] W. Shin, T. Yasuda, G. Watanabe, Y.S. Yang, C. Adachi, Chem. Mat. 25 (2013) 2549.
[11] C. Cui, J. Min, C.-L. Ho, T. Ameri, P. Yang, J. Zhao, C.J. Brabec, W.-Y. Wong, Chem. Commun. 49 (2013) 4409.
[12] J. Zhou, X. Wan, Y. Liu, Y. Zuo, Z. Li, G. He, G. Long, W. Ni, C. Li, X. Su, Y. Chen, J. Am. Chem. Soc. 134 (2012) 16345.
[13] J. Zhou, Y. Zuo, X. Wan, G. Long, Q. Zhang, W. Ni, Y. Liu, Z. Li, G. He, C. Li, B. Kan, M. Li, Y. Chen, J. Am. Chem. Soc. 135 (2013) 8484.
[14] N.D. Eisenmenger, G.M. Su, G.C. Welch, C.J. Takacs, G.C. Bazan, E.J. Kramer, M.L. Chabinyc, Chem. Mat. 25 (2013) 1688.
[15] C.M. Amb, S. Chen, K.R. Graham, J. Subbiah, C.E. Small, F. So, J.R. Reynolds, J. Am. Chem. Soc. 133 (2011) 10062.
[16] J. Zhou, X. Wan, Y. Liu, G. Long, F. Wang, Z. Li, Y. Zuo, C. Li, Y. Chen, Chem. Mat. 23 (2011) 4666.
[17] H.J. Son, W. Wang, T. Xu, Y. Liang, Y. Wu, G. Li, L. Yu, J. Am. Chem. Soc. 133 (2011) 1885.
[18] Y. Sun, G.C. Welch, W.L. Leong, C.J. Takacs, G.C. Bazan, A.J. Heeger, Nat. Mater. 11 (2012) 44.
[19] F. Silvestri, A. Marrocchi, M. Seri, C. Kim, T.J. Marks, A. Facchetti, A. Taticchi, J. Am. Chem. Soc. 132 (2010) 6108.
[20] M. Seri, A. Marrocchi, D. Bagnis, R. Ponce, A. Taticchi, T.J. Marks, A. Facchetti, Adv. Mater. 23 (2011) 3827.
[21] R. Grisorio, G. Allegretta, G.P. Suranna, P. Mastrorilli, A. Loiudice, A. Rizzo, M. Mazzeo, G. Gigli, J. Mater. Chem. 22 (2012) 19752.
[22] J.-W. Mun, I. Cho, D. Lee, W.S. Yoon, O.K. Kwon, C. Lee, S.Y. Park, Org. Electron. 14 (2013) 2341.
[23] P.M. Beaujuge, J.M.J. Fréchet, J. Am. Chem. Soc. 133 (2011) 20009.
[24] R. Fitzner, C. Elschner, M. Weil, C. Uhrich, C. Körner, M. Riede, K. Leo, M. Pfeiffer, E. Reinold, E. Mena-Osteritz, P. Bäuerle, Adv. Mater. 24 (2012) 675.
[25] A. Marrocchi, F. Silvestri, M. Seri, A. Facchetti, A. Taticchi, T.J. Marks, Chem. Commun. 49 (2009) 1380.
[26] M.T. Lloyd, A.C. Mayer, A.S. Tayi, A.M. Bowen, T.G. Kasen, D.J. Herman, D.A. Mourey, J.E. Anthony, G.G. Malliaras, Org. Electron. 7 (2006) 243.
[27] J. Sun, J.-G. Cheng, W.-Q. Zhu, S.-J. Ren, H.-L. Zhong, D.-L. Zeng, J.-P. Du, E.-J. Xu, Y.-C. Liu, Q. Fang, J. Polym. Sci. Pol. Chem. 46 (2008) 5616.
[28] W. Cui, Y. Zhao, H. Tian, Z. Xie, Y. Geng, F. Wang, Macromolecules 42 (2009) 8021.
[29] J. Sun, H. Zhong, E. Xu, D. Zeng, J. Zhang, H. Xu, W. Zhu, Q. Fang, Org. Electron. 11 (2010) 74.
[30] X. Li, X. Zhang, W. Li, Y. Wang, T. Liu, B. Zhang, W. Yang, J. Mater. Chem. 21 (2011) 3916.
[31] H.C. Zhang, E.Q. Guo, Y.L. Zhang, P.H. Ren, W.J. Yang, Chem. Mat. 21 (2009) 5125.
[32] R. Giménez, M. Piñol, J.L. Serrano, Chem. Mat. 16 (2004) 1377.
[33] S.Y. Jo, J. Shin, S.Y. Bae, K.H. Kim, T.W. Lee, S.-H. Son, K.-K. Kim, D.H. Choi, Synth. Met. 161 (2011) 833.
[34] J.A. Hur, S.Y. Bae, K.H. Kim, T.W. Lee, M.J. Cho, D.H. Choi, Org. Lett. 13 (2011) 1948.
[35] J. Shin, N.S. Kang, K.H. Kim, T.W. Lee, J.-I. Jin, M. Kim, K. Lee, B.K. Ju, J.-M. Hong, D.H. Choi, Chem. Commun. 48 (2012) 8490.
[36] K.P. Pernstich, S. Haas, D. Oberhoff, C. Goldmann, D.J. Gundlach, B. Batlogg, J. Appl. Phys. 96 (2004) 6431.
[37] C.R. Newman, C.D. Frisbie, D.A. da Silva Filho, J.-L. Brédas, P.C. Ewbank, K.R. Mann, Chem. Mat. 16 (2004) 4436.
[38] B. Walker, A.B. Tamayo, X.-D. Dang, P. Zalar, J.H. Seo, A. Garcia, M. Tantiwiwat, T.-Q. Nguyen, Adv. Funct. Mater. 19 (2009) 3063.
[39] L. Chang, H.W.A. Lademann, J.-B. Bonekamp, K. Meerholz, A.J. Moulé, Adv. Funct. Mater. 21 (2011) 1779.
[40] J.A. Mikroyannidis, D.V. Tsagkournos, S.S. Sharma, Y.K. Vijayc, G.D. Sharma, J. Mater. Chem. 21 (2011) 4679.
[41] G. Li, V. Shrotriya, J. Huang, Y. Yao, T. Moriarty, K. Emery, Y. Yang, Nat. Mater. 4 (2005) 864.
[42] C.V. Hoven, X.-D. Dang, R.C. Coffin, J. Peet, T.-Q. Nguyen, G.C. Bazan, Adv. Mater. 22 (2010) E63.
[43] W.-R. Wu, U.-S. Jeng, C.-J. Su, K.-H. Wei, M.-S. Su, M.-Y. Chiu, C.-Y. Chen, W.-B. Su, C.-H. Su, A.-C. Su, ACS Nano 8 (2011) 6233.
[44] W. Chen, T. Xu, F. He, W. Wang, C. Wang, J. Strzalka, Y. Liu, J. Wen, D.J. Miller, J. Chen, K. Hong, L. Yu, S.B. Darling, Nano Lett. 11 (2011) 3707.
[45] T. Agostinelli, S. Lilliu, J.G. Labram, M. Campoy-Quiles, M. Hampton, E. Pires, J. Rawle, O. Bikondoa, D.D.C. Bradley, T.D. Anthopoulos, J. Nelson, J.E. Macdonald, Adv. Funct. Mater. 21 (2011) 1701–1708.
[46] R.I. Gearba, T. Mills, J. Morris, R. Pindak, C.T. Black, X. Zhu, Adv. Funct. Mater. 21 (2011) 2666.
[47] G.C. Welch, L.A. Perez, C.V. Hoven, Y. Zhang, X.-D. Dang, A. Sharenko, M.F. Toney, E.J. Kramer, T.-Q. Nguyen, G.C. Bazan, J. Mater. Chem. 21 (2011) 12700.
[48] C. Melzer, E.J. Koop, V.D. Mihailetchi, P.W.M. Blom, Adv. Funct. Mater. 14 (2004) 865.
[49] S. Günes, H. Neugebauer, N.S. Sariciftci, Chem. Rev. 107 (2007) 1324.
[50] P. Dutta, H. Park, W.-H. Lee, I.-N. Kang, S.-H. Lee, Org. Electron. 13 (2012) 3183.